Exploring Physical and Chemical Properties in new Multifunctional Indium, Bismuth and Zinc based 1D and 2D Coordination Polymers

Article *in* Dalton Transactions · December 2017

DOI: 10.1039/C7DT04287F

CITATIONS
2

READS
237

16 authors, including:

German E. Gomez
Karlsruhe Institute of Technology
26 PUBLICATIONS **98** CITATIONS
SEE PROFILE

Richard Fernando D'vries
Universidad Santiago de Cali
56 PUBLICATIONS **374** CITATIONS
SEE PROFILE

Diego Fernando Lionello
Comisión Nacional de Energía Atómica
9 PUBLICATIONS **17** CITATIONS
SEE PROFILE

Lina María Aguirre Díaz
Instituto de Ciencia de Materiales de Madrid
23 PUBLICATIONS **222** CITATIONS
SEE PROFILE

Dalton Transactions

Accepted Manuscript

This article can be cited before page numbers have been issued, to do this please use: G. Gómez, R. F. D'Vries, D. F. Lionello, L. M. Aguirre Diaz, M. Spinosa, C. Costa, M. C. Fuertes, R. A. Pizarro, A. M. M. Kaczmarek, J. A. Ellena, L. ROZES, M. Iglesias, R. Van Deun, C. Sanchez, A. Monge and G. Soler Illia, *Dalton Trans.*, 2017, DOI: 10.1039/C7DT04287F.

This is an Accepted Manuscript, which has been through the Royal Society of Chemistry peer review process and has been accepted for publication.

Accepted Manuscripts are published online shortly after acceptance, before technical editing, formatting and proof reading. Using this free service, authors can make their results available to the community, in citable form, before we publish the edited article. We will replace this Accepted Manuscript with the edited and formatted Advance Article as soon as it is available.

You can find more information about Accepted Manuscripts in the author guidelines.

Please note that technical editing may introduce minor changes to the text and/or graphics, which may alter content. The journal's standard Terms & Conditions and the ethical guidelines, outlined in our author and reviewer resource centre, still apply. In no event shall the Royal Society of Chemistry be held responsible for any errors or omissions in this Accepted Manuscript or any consequences arising from the use of any information it contains.

ROYAL SOCIETY OF CHEMISTRY

rsc.li/dalton

View Article Online
DOI: 10.1039/C7DT04287F

Journal Name

ARTICLE

Exploring Physical and Chemical Properties in new Multifunctional Indium, Bismuth and Zinc based 1D and 2D Coordination Polymers

Received 00th January 20xx,
Accepted 00th January 20xx

DOI: 10.1039/x0xx00000x

www.rsc.org/

G. E. Gomez,[a,b*] R. D'Vries,[c,d*] D. F. Lionello,[a,e] L. M. Aguirre-Díaz,[f] M. Spinosa,[g] C. S. Costa,[h] M. C. Fuertes,[a,e] R. A. Pizarro,[h] A. M. Kaczmarek,[i] J. Ellena,[d] L. Rozes,[j] M. Iglesias,[f] R. Van Deun,[i] C. Sanchez,[j*] M. A. Monge[f] and G. J. A. A. Soler Illia[b*]

Main group elements coordination polymers (MGE-CPs) are important compounds for the development of multifunctional materials. However, studies regarding to structural, optical, catalitic, mechanical or antibacterial properties have strikingly less reported. In this work, an exhaustive study of a set of crystalline MGE-CPs obtained from bismuth and indium metals, iminodiacetate, 1,2,4,5-benzenetetracarboxylate, and 2,2'-bipyridine as building blocks is presented. An in-deep topological analysis of the networks was carried out. Besides, nanoindentation studies were performed on two representative low dimensional compounds in order to find the relationships between their structural features and the intrinsic mechanical properties (hardness and elasticity). The solid state photoluminescence (SSPL) properties were also studied in terms of excitation, emission, lifetimes values and CIE chromaticites. Moreover, the heterogeneous catalytic activities of the compounds were evaluated in the cyanosilylation reaction using a set of carbonylic substrates under solvent-free conditions. Finally, the inhibitory effect of the Bi-CPs on the growth of microorganisms such as *Escherichia coli*, *Salmonella enterica* serovar Typhimurium and *Pseudomonas aeruginosa*, which are associated with relevant infectious diseases, is reported.

Introduction

Inorganic–organic hybrid compounds as coordination polymers (CPs) or Metal Organic Frameworks (MOFs) have becoming the focus of research due to its unique properties such as gas sorption,[1] optics[2] and heterogeneous catalysis.[3] In comparison with transition metals from d and f block, the main group elements (MGE) were less explored for designing new coordination compounds. In the last years most of metal ions have been incorporated into these materials, but only recently Bi^{3+}-compounds with optical[4] or catalytic[5] properties have been reported. For this reason, the synthesis and studies related to Bi-CPs is surprisingly scarce.

Particularly, our research has been addressed on the synthesis of new CPs and MOFs with optical,[6] mechanical,[7] catalytic,[8,9,10] thermo[8,11], chemical[6b] and sensing properties[12] exploring the structure-property relationships. Moreover, the catalytic properties of In-CPs have been widely explored by Monge's group finding exceptional correlations between the structures and its catalytic performances.[13]

Because of its geometrically flexible coordination environments, the trivalent Bi ion can be regarded as a novel node in the construction of CPs. Moreover, bismuth leads to unpredictable and diverse of structures since it presents a variety of coordination numbers. In this context, Inge et al. [14] recently reported an 8-coordinated Bi-MOF constructed from a tricarboxylate linker, revealing an unprecedented topological complexity.

From the point of view of the design of new CPs, during last decade iminodiacetic and 1,2,4,5-benzenetetracarboxylic acids have been employed as building blocks for the synthesis of CPs and MOFs as multifunctional platforms[15].

[a] Gerencia de Química, Centro Atómico Constituyentes, Comisión Nacional de Energía Atómica, Av. Gral. Paz 1499, 1650 San Martin, Buenos Aires, Argentina. *E-mail: gegomez@unsl.edu.ar
[b] Instituto de Nanosistemas. Universidad Nacional de San Martín. Av. 25 de Mayo 1021, San Martín, Buenos Aires, Argentina.
[c] Facultad de Ciencias Básicas, Universidad Santiago de Cali, Calle 5 # 62-00, Cali, Colombia. *E-mail: gsoler-illia@unsam.edu.ar
[d] Instituto de Física de São Carlos, Universidade de São Paulo, CP. 369, 13560-970, São Carlos - SP, Brasil. *E-mail: richard.dvries00@usc.edu.co
[e] Instituto Sabato, UNSAM-CNEA, Av. Gral. Paz 1499, B1650KNA San Martín, Buenos Aires, Argentina.
[f] Departamento de Nuevas Arquitecturas en Química de Materiales, Materials Science Factory, Instituto de Ciencia de Materiales de Madrid–Consejo Superior de Investigaciones Científicas, Sor Juana Inés de la Cruz 3, Madrid 28049, Spain.
[g] Programa Nacional de Gestión de Residuos Radiactivos-PNGRR, Comisión Nacional de Energía Atómica, Av. Gral. Paz 1499, 1650 San Martin, Buenos Aires, Argentina.
[h] Departamento de Radiobiología, Gerencia de Química Nuclear y Ciencias de la Salud, Comisión Nacional de Energía Atómica, Av. Gral. Paz 1499, 1650 San Martin, Buenos Aires, Argentina.
[i] L^3 – Luminescent Lanthanide Lab, Ghent University, Department of Chemistry, Krijgslaan 281, Building S3, 9000 Gent, Belgium.
[j] UMR 7574 Chimie de la Matière Condensée de Paris, UPMC Univ. Paris 06-CNRS, Collège de France, 11 place Marcelin Berthelot, 75231, Paris Cedex 05, France. *E-mail: clement.sanchez@upmc.fr

Electronic Supplementary Information (ESI) available: Electronic supplementary information (ESI) available: Synthetic procedure details, experimental X-ray powder patterns, TGA and DSC profiles, FTIR spectra and decay luminescence profiles. CCDC 1561408–1561411. See DOI: 10.1039/x0xx00000x

View Article Online
DOI: 10.1039/C7DT04287F

On the other hand, diverse strategies have been proposed to overcome the increasing antibiotic resistance observed in several pathogenic microorganisms.[16] In this sense, due their novel physicochemical properties, metallic or oxides nanoparticles (NPs) have been developed to counteract microbial pathogens.[16] In the case of Bi, different compounds are being used against ulcers and treatments of gastritis, diarrhoea and dyspepsia.[17] Moreover, bismuth derivatives (for example bismuth subsaliciylate and bismuth citrate) have been used long before as antimicrobial agents against several bacterial species, particularly *Helycobacter pylori*, a bacterium responsible for peptic ulcer and gastric cancer[17e]. Their antimicrobial activity were observed at relatively high concentrations due to their limited water solubility.[17] In addition, it has been demonstrated that Bi-NPs reduce biofilm (growth of microorganisms on solid surfaces) formation in bacteria and fungus such as *Streptococcus mutans* and *Candida albicans.*[19,20] Biofilms represent a great problem for industry and human health because they form on a wide variety of surfaces, possess high resistance to antimicrobial agents and are very difficult to eradicate.[21]

Besides, to understand the processability and the mechanical properties of the new materials, nanoindentation studies have recently been adopted. Thanks to pioneering work of Cheetham[22], nanoindentation tests have been applied to demonstrate the intrinsic correlations between the crystal packing and the anisotropic mechanical properties (such as density, stability and elasticity) in MOF materials.

The present work involves a complete study regarding the synthesis strategies, photophysical characterization, mechanical and catalytic analysis and antimicrobial activity of a set of CPs based in main-group elements (MGE-CPs), more specifically two Bi-CPs and one In-CP.

2.0. Experimental section

2.1. Synthesis: [Bi(1,2,4,5-BTC)$_{0.5}$(2,2'-bipyridine)(NO_3)(DMF)] (**Bi-1**), [Bi(IDA)(IDAH)] (**Bi-2**), [In(IDA)(Cl)] (**In-1**) and [Zn(1,2,4,5-BTC)$_{0.5}$(2,2'-bipyridine)(H_2O)] (**Zn-1**), were obtained as crystalline solids under solvothermal conditions using 43 mL Teflon-lined Parr reactors. The solid reactants and solvents were used as received without purification from Across Organics (1,2,4,5-benzenetetracarboxylic acid) and Sigma-Aldrich (2,2'-bipyridine, $Bi(NO_3)_3{\cdot}5H_2O$, N,N'-dimethylformamide, iminodiacetic acid, $Zn(NO_3)_2{\cdot}6H_2O$ and $InCl_3$) (see SI section S1 for synthesis details).

2.2. Fourier transform infrared spectroscopy (FTIR): FTIR spectra were recorded with a Nicolet Protégé 460 spectrometer in the 4000-400 cm^{-1} range with 64 scans and a spectral resolution of 4 cm^{-1} by the KBr pellet technique. The FTIR spectra and band assignments are displayed in SI section S2.

2.3. Thermal Analysis: Thermogravimetric Analysis (TGA) and Differential Scanning Calorimetry (DSC) were performed with Shimadzu TGA-51 and DSC-60 apparatus under flowing air at 50 mL min^{-1}, at a heating rate of 10 °C min^{-1}. TGA and DSC curves are displayed in SI section S3.

2.4. Powder X-ray diffraction (PXRD): PXRD patterns were obtained with a Rigaku D-MAX-IIIC diffractometer using CuKα radiation (λ1= 1.54056 Å, λ2= 1.54439 Å) (see SI section S4).

2.5. Scanning electron microscopy (SEM): SEM micrographs and Energy Dispersive Spectroscopy (EDS) (SI section S5) were obtained with FEI Quanta 200 equipment. Samples were placed on an adhesive carbon tape coated with gold for the observations.

2.6. Single-Crystal structure determination (SCXRD). SCXRD data for compounds **Bi-1**, **Bi-2** and **Zn-1** were collected at room temperature (293 K) on a Rigaku XTALAB-MINI diffractometer using MoKα radiation (0.71073 Å) monochromated by graphite. **In-1** compound was collected at room temperature (296 K) on a Bruker APEX-II CCD diffractometer using MoKα radiation (0.71073 Å) monochromated by graphite.

The cell determination and the final cell parameters of **Bi-1**, **Bi-2** and **Zn-1** were obtained on all reflections using the software *CrystalClear*.[23] Data integration and scaled was carried out using the software *CrystalClear*[23] and *CrysAlisPro*.[24] The structures were solved and refinement with SHELXS-2013[25] software, included in WinGX[26] and Olex2.[27] Cell determination and final cell parameters of **In-1** crystals were obtained on all reflections using the software Bruker SAINT included in APEX2 software suite.[28] Data integration and scaled was carried out using the software Bruker SAINT.[27] In all cases non-hydrogen atoms of the molecules were clearly resolved and full-matrix least-squares refinements of these atoms with anisotropic thermal parameters were performed. Besides, hydrogen atoms were stereochemically positioned and refined by the riding model.[25] ORTEP diagrams for all structures were prepared with Diamond.[29] TOPOS[30] and Mercury[31] programs were used in the preparation of the artwork of the polyhedral and topological representations.

2.7. Mechanical characterization: samples were prepared for mechanical characterizations including single crystals in acrylic resin (SUBITON®). Nanoindentation (NI) experiments were performed using an Agilent G200 Nano Indenter at room temperature. A Berkovich diamond tip with a final rounding of 20 nm was used in this study. The tip was calibrated using a standard fused silica sample. A group of 5 crystals were tested, an array of 5x5 measurements up to a maximum penetration depth of 1200 nm were carried out on each selected crystal. Elastic modulus (E) and hardness (H) were calculated from the measurements applying the Oliver & Pharr model, described in our previous work.[7]

2.8. Solid State Luminescence Measurements: The steady state and time resolved luminescence measurements were performed on an Edinburgh Instruments FLSP920 spectrometer setup, using a 450 W xenon lamp as the steady state excitation source and an EPLED as the time resolved excitation source with a fixed excitation wavelength of 331 nm. The emission was detected by a Hamamatsu R928P PMT photomultiplier tube. Excitation spectra were corrected for the xenon lamp emission profile, whereas emission spectra were corrected for the detector response curve. All measurements were carried out at a step size of 1 nm.

View Article Online
DOI: 10.1039/C7DT04287F

2.9. Catalytic Activity: Considering the nature of the new materials, among all possible organic transformations, only those which require a Lewis acid as catalyst, were taken into account. So, as a standard organic transformation the cyanosilylation reaction was chosen in order to evaluate the catalytic activity of **Bi-1**, **Bi-2** and **In-1** materials. In this order, catalytic amounts of the selected material (0.5mol %, 1mol % and 2.5mol %) were placed in a Schlenk tube under nitrogen atmosphere without solvents, together with the corresponding carbonyl compound (1 equivalent); trimethylsilyl cyanide (1.1 equivalent) was then added dropwise by syringe. The mixture was stirred until disappearance of the carbonyl compound; the kinetics of the reaction and its yield were checked by GC-MS.

3.0. Antibacterial assays.

3.0.1. Stock solutions of bismuth compounds

Saturated aqueous solutions of the relatively insoluble compounds **Bi-1**, **Bi-2** and Bismuth citrate (Bi-cit) (Merck) were prepared in distilled and sterilized water by 0.22-µm-pore-size filters. Bi-cit was employed as control because, which is known as a bismuth derivative inhibitor of bacterial growth[16b]. The concentrations of bismuth compounds were expressed as elemental bismuth determined by Total Reflection X-ray Fluorescence Spectrometry (PicoFox S2 TXRF – Bruker). Bi-NPs and Bi-cit concentrations used for this study depended on their limited water solubility.

3.0.2. Bacterial strains and growth conditions. The employed set of bacteria were *Escherichia coli* (*E. coli*, strain K12), *Salmonella enteric* serovar Typhimurium (S. Typhimurium, strain LT2) and *Pseudomonas aeruginosa* (P. aeruginosa, strain PAO1). For assays with planktonic (free) cells, *E. coli*, *S. Typhimurium* and *P. aeruginosa* were cultivated in Nutrient Broth (Difco) at a temperature of 37 °C. For biofilm assays, *P. aeruginosa* was grown in LB broth (10 g tryptone, 5 g yeast extract and 5 g NaCl in 1000 ml distilled water) at 37 °C.

3.0.3. Effect of Bi-NPs on planktonic cultures and biofilm formation. For assays with planktonic cultures, sterile Bi-compounds were serially suspended in tubes containing 1 milliliter of Nutrient Broth. Overnight cultures of the three bacterial strains were diluted 1/100 in saline solution and 100 µl were added to each prepared tube as described. The tubes were incubated for 24 h at 37 °C. Cell mass was evaluated by optical density at 650 nm wavelength (OD_{650}). Quantification of viable microorganisms was determined by plate count in Nutrient Agar (Difco) at 37 °C and expressed by colony forming units per ml (CFU/ml). Tubes without Bi-compounds were used as control. For studies of biofilm formation, overnight cultures of *P. aeruginosa* were diluted 1/100 in LB in a final volume of 100 µl in absence or presence of different concentrations of Bi-compounds in 96-well microplates. After 24 h incubation at 37 °C in a moist chamber, planktonic cells were discarded and biofilm attached to the surface of microplate wells was quantified by the "method of crystal violet stain".[32]

4.0. Results

4.1. Synthesis

After the followed procedure detailed in (Scheme 1), the phases were characterized by PXRD and EDS in order to confirm their purity (see SI section S4 and S5). The morphologies diversity was studied by SEM; plate habits were identified in **Bi-1**, **Bi-2** and **Zn-1** meanwhile **In-1** exhibited cubic crystals (Figure 1). Good quality crystals were carefully selected in order to perform SCXRD. The exhibited table in SI section S6 summarizes the crystallographic data for all the synthesized compounds.

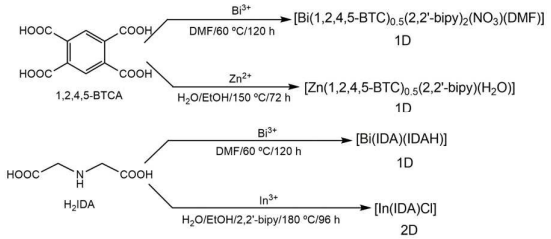

Scheme 1: Synthesis of the reported CPs.

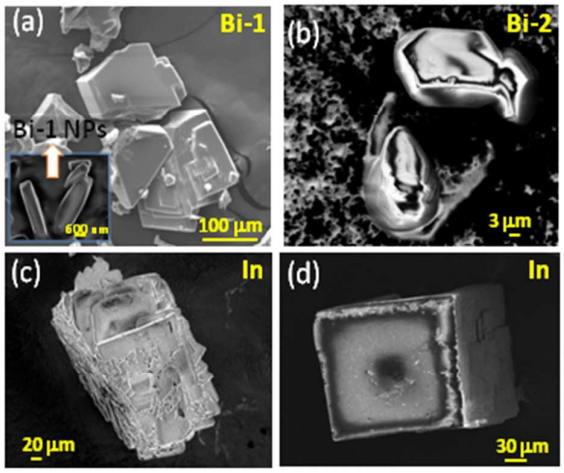

Figure 1: Micrographs of **Bi-1** (a), **Bi-2** (b) and **In-1** obtained with (d) and without (c) growth modulator.

4.2. Crystal Structure Descriptions

Bi-1 compound crystallizes in the triclinic *Pī* space group. The primary building unit (PBU) consists in a nine-coordinated arrangement (BiO_7N_2), where seven oxygen atoms belonging to 1,2,4,5-BTC, DMF and nitrate, and two nitrogen atoms from the 2,2'-bipyridine form a trigonal prism square-face tricapped polyhedron (TPRS-9)[33] (Figure 2 left). As can been seen in Figure 2 (right), the asymmetric unit of **Bi-1** is composed by one trivalent Bi cation, one nitrate anion, one DMF and one 2,2'-bipyridine; in addition to a half of a crystallographically independent 1,2,4,5-BTC ligand.

In this compound each 1,2,4,5-BTC ligand is coordinated to four Bi centers in chelate η^2 mode, giving rise to chains along [1 0 0] direction (Figure 3 left) with a intermetallic distances of 6.3594(6) and 9.3852(7) Å. The Bi-O bond lengths are in the

View Article Online
DOI: 10.1039/C7DT04287F

range 2.326(5)-2.77(1) Å as it was seen in analogous Bi-MOFs.[14]

The crystal structure of **Bi-1** was analyzed with TOPOS program in order to determine the underlying topology[34] of the associated simplified net. Through this simplification it is possible to observe that the carboxylate ligand acts as 4-connected node and the metal center acts as bridge forming "ribbon-like" chains (Figure 3 left). In addition, the compound can be classified as I^0O^1 according to the proposed classification suggested by Cheetham *et al.*[35] describing "coordination polymeric chains".

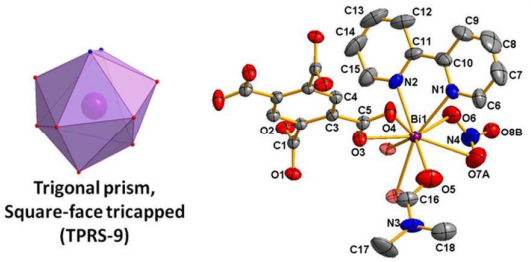

Figure 2: Polyhedron representation of the PBU (left) and 50% of probability thermal ellipsoids diagram showing for **Bi-1** (right). Hydrogen and disordered atoms were omitted for clarity.

The 3D supramolecular structure (Figure 3) is based on weak hydrogen bonds that join the chains along [0 1 0] and [0 0 1] directions, with distances C9-H9···O6 = 3.248(1) and C18-H18A···Cg = 3.460(2) Å, respectively (Cg ring = C2, C3, C4, C2*, C3*, C4*).

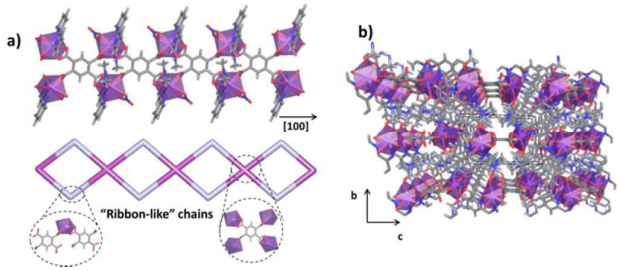

Figure 3: a) Polymeric chain and decorated simplified chain along [1 0 0] direction and b) crystal packing view into *bc* plane of **Bi-1** compound.

For comparative purposes **Zn-1** compound[36,37] was obtained. A deeper crystallographic description can been found in SI section S7. Similarly to **Bi-1**, here the 1,2,4,5-BTC ligand is coordinated to four metallic centers giving rise to "ribbon-like" chains along [1 0 0] direction with intermetallic distances of 7.6958(7) and 8.0797(8) Å (Figure 4 a). Despite presenting different coordination number, both compounds exhibit similar arrangement of the ligand giving rise to 1D coordination polymers.

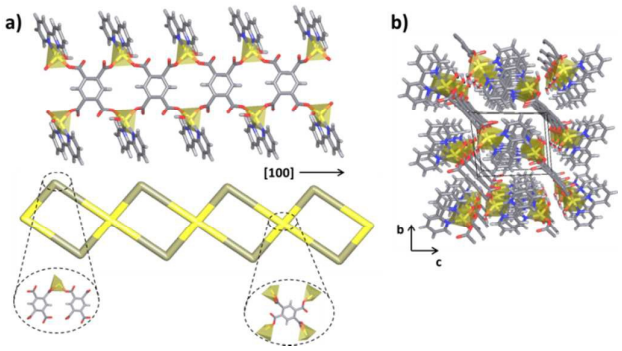

Figure 4: a) Polymeric chain and decorated simplified chain along [1 0 0] direction and b) crystal packing view into *bc* plane of **Zn-1** compound.

Bi-2 was obtained as a crystalline solid belonging to monoclinic *C2/c* space group. The asymmetric unit is formed by one crystallographically independent trivalent Bi cation and two structurally different types of iminodiacetate ligand (IDA and protonated IDAH). The PBU can be described as 8-coordinated metal center (BiO_7N) formed by seven oxygens and one nitrogen atom from the ligands, forming a square antiprism polyhedron (SAPR-8) arrangement. In this case, the metal centers are joined by the ligand forming dimmeric sharing edge SBUs ($Bi_2N_2O_{12}$) with a intermetallic distance of 3.9612(9) Å. The formation of the dimmeric SBUs is due to $\mu\eta_2$ and $\mu_2\eta_2$ coordination modes of the carboxylate groups respectively (see SI section S8).

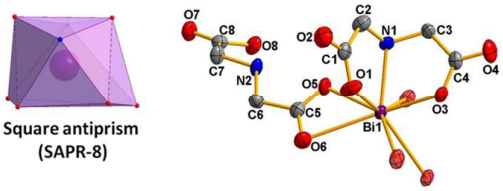

Figure 5: PBU representation of the Bi^{3+} cation (left) and 50% of probability thermal ellipsoids diagram showing for **Bi-2** (right). Hydrogen and disordered atoms were omitted for clarity.

In the extended structure the IDA acts as tridentated ligand blocking the coordination sphere of the Bi^{3+}, while the IDAH ligand join the SBUs along [0 0 1] direction giving rise to "ribbon-like" chains (Figures 5 left and SI section S8). Besides the IDAH ligands join two metallic centers forming dimmeric SBUs, acting as 4-connected nodes. The 3D supramolecular crystal packing (Figure 5 right) is given by hydrogen bonds along [1 0 0] direction with distances N1-H1···O4 = 2.932(6) and C2-H2C···O2 = 3.175(8) Å. Similar interactions are involved along [0 1 0] direction with distances N2-H2B···O2 = 2.908(7) and N2-H2A···O4 = 3.091(6) Å.

View Article Online
DOI: 10.1039/C7DT04287F

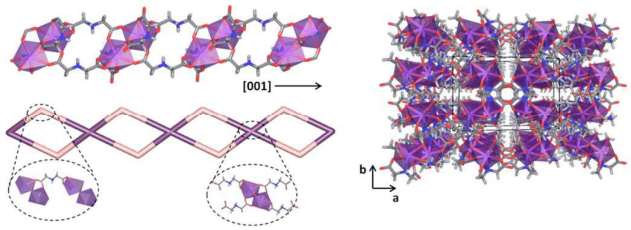

Figure 6: Polyhedron and simplified representation of the chains (left) and crystal packing view along [0 0 1] direction of **Bi-2** (right).

The 3D supramolecular structure is formed by strong hydrogen bonds and π-π stacking interactions with distances O5-H5A···O1 = 2.657(3) and Cg...Cg = 3.758(2) Å, along [0 0 1] and [0 1 0] directions respectively.

In-1 crystallizes in the *Pnma* orthorhombic space group. The metal environment is formed by one Cl atom, one nitrogen and four oxygen atoms, giving rise to a distorted octahedral geometry (Figure 6 left). The asymmetric unit is formed by a half of In^{3+} cation, chloride anion and IDA ligand. The ORTEP diagram of **In-1** is displayed in the Figure 7 right. Each ligand is coordinated in μ_3 chelate fashion through the protonated nitrogen atom and two oxygen atoms of the carboxylate group. Beside the carboxylate groups exhibits $\mu\eta^2$ coordination mode linking a pair of metallic centers (intermetallic distance = 5.645(2) Å) along [0 1 1] and [0 -1 -1] directions (Figure 8).

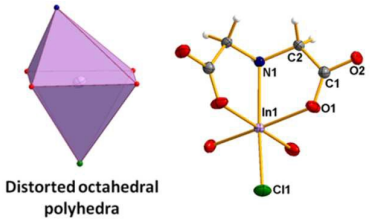

Figure 7: Polyhedron representation of the In^{3+} (left) and 50% of probability thermal ellipsoids diagram showing for **In-1** compound (right).

The junction of the metallic centers gives rise to layers in the (011) plane. As far as we know, this structure was topologically analyzed by first time. In this case each metal acts as 4-connected node joined by the ligand forming a **sql**/Shubnikov topology net with point symbol ($4^4.6^2$) (Figure 8b). The 3D supramolecular structure is formed by the Cl···H-N interaction with a distance of 2.719(6) Å which enables the stacking of the covalent layers along [1 0 0] direction (Figure 8c).

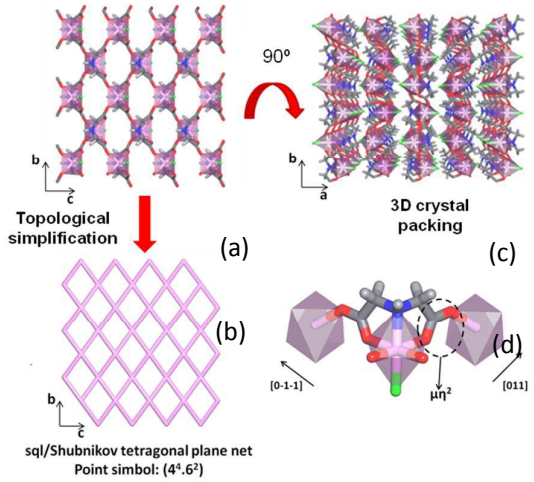

Figure 8: Representation of the 2D covalent network (a), topological simplification (b), 3D crystal packing (c) and the coordination modes of the IDA ligand in **In-1** (d).

4.3. Nanomechanical properties

Dense CPs incorporate infinite inorganic connectivity, especially those based on metal-oxygen-metal motifs. During last years, there has been an intense interest focused on CPs showing unique physical properties associated with their structures, which includes magnetic, electrical, optical and multiferroic properties. In spite of that, studies inherent with mechanical features of CPs are scarce. Besides, for developing MOFs/CPs sensing devices, it is required good film stiffness and film-to-substrate adhesion strength. Moreover, elastic properties of the underlying framework are dominant in the performance of piezoelectric devices (such as actuators and sensors) and MOFs coatings or membranes.[38]

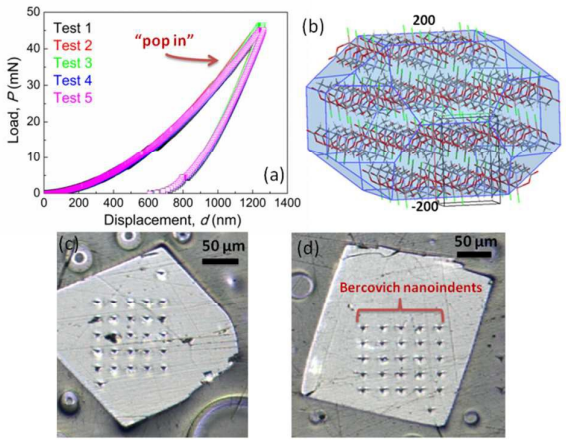

Figure 9: *P–h* profiles (a) of **In-1** crystals. Studied planes, in normal direction to the nanoindenter (b). Indented cube crystals (c and d).

In this context, it was highlighted the special interest for the mechanical characterization of low dimensional 1D or 2D frameworks due to the possibility of delamination ("top-down"

View Article Online
DOI: 10.1039/C7DT04287F

fabrication) and further deposition onto different substrates to build membranes and thin-films composites.[39,40] To elucidate structural-mechanical properties, NI experiments were performed on selected single crystals of **In-1** and **Bi-2** as representative models (Figures 9a and 10a). In both cases, a 5x5 field of NI was applied on the single crystals. With the purpose of avoid ambiguities, NI experiments on the acrylic substrate were made (see displacement (*P-h*) curves in SI section S9) as a control experiment, obtaining H and E values of 0.11±0.01 and 2.8±0.1 GPa respectively.

The crystallographic planes which probabilistically are exposed in **In-1** compound, also coincident to those which divides the nanolayers, are the family of *h00* ones. In SI section S1, it is clear to identify a preferential orientation into the [2 0 0] planes. These planes are exposed by deposition of the layers, which are located the direction in which non-covalent interactions ensure the packing of the layers (see Figure 9b). The same family of 200 planes in **Bi-2** (Figure 10b) exposes a higher concentration of metallic polyhedral, conferring *structural stiffness*. As can be seen in Figure 9 and 10 c and d, the "Berkovich marks" were identified after NI measurements.

The averages values of H and E measured for **In-1** were 1.8±0.1 GPa and 24.3±0.8 GPa, respectively, and for **Bi-2** were and 1.1±0.1 GPa and 12.4±0.5 GPa. The obtained values from **Bi-2** are considerably lower compared to **In-1**, possibly due to a decrease in stiffness for being a one-dimensional.

It is important to note the presence of "pop-in", or displacement events, in the NI performed experiments, which appears due to the breakages of intermolecular weak bonds. Similar displacements have been reported in low-dimensional CPs such as $[Yb_2(3\text{-}OHNDS)_2(1,10\text{-}phen)_2(H_2O)]\cdot 3H_2O$[7], $[Cu(H_2O)_2(O_3PCH_2CO_2)_2]$[41] and [Mn(2,2-dms)][40].

According to the classification reported by Cheetham and colleagues[42], **In-1** was located into the "dense hybrids" type materials and close to MOFs with similar mechanical performance (SI section 10).

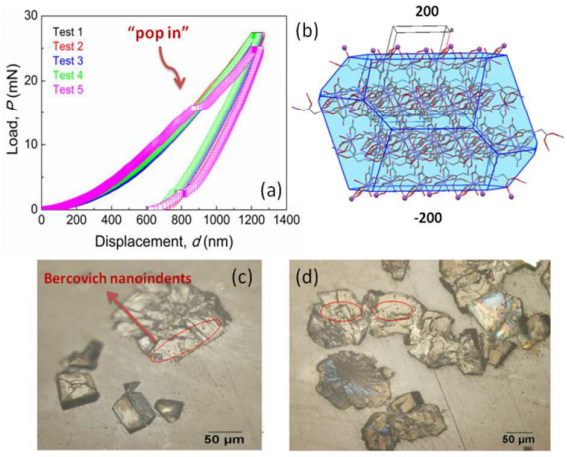

Figure 10: *P–h* profiles (a) of **Bi-2** crystals. Studied planes, in normal direction to the nanoindenter (b). Indented single crystals (c and d).

4.4. Solid-state photoluminescent properties (SSPL)

According to a significant number of specialized articles[2] about photoluminescent (PL) properties, optical materials can be characterized by specific studies: (1) emission spectra (recorded as intensity *vs* wavelength), (2) quantum yields (QYs), and (3) the observed lifetime (τ_{obs}) which refer to the efficiency of the luminescence process and the average time the molecule stays in its excited state before emitting a photon, respectively.

In contrast to the narrow and well predictable emissions of 4f-4f transitions in rare earths elements[43], the PL in transition metals and MGE commonly exhibits broad bands. The excited states in TM and MGE-based compounds are different from the ground state and, often, considerably anti-bonding producing broad emissions and large stokes shifts. Besides, many types of PL might occur in the same compound, being a challenge the identification of the electronic transitions.

LMCT (ligand to metal charge transition) might occur in TM and MGE-CPs with metals in high oxidation states, nevertheless the assignment of LMCT in these compounds is often difficult, especially in mixed ligand systems. On the other hand, the most likely candidates for metal-centered emission are CPs containing s^2-ions such Pb^{2+} and Bi^{3+}, where it is possible to observe s-p transitions[44].

The SSPL properties of **Bi-1**, **Bi-2** were studied by recording excitation-emission spectra, calculating lifetime values and quantificating the color emission (QC) in comparison with the respective starting reactants ($Bi(NO_3)_3$, H_2IDA and H_4BTC). Usually, the spectroscopy of Bi^{3+} with s^2 configuration in the ground state and sp configuration in the first excited state is discussed in Russell–Saunders-type electronic energy terms. Intense fluorescent emissions could be assigned to LMCT or the $^1P_1 \leftarrow {}^1S_0$ and $^3P_1 \leftarrow {}^1S_0$ transitions of the s^2 electron of trivalent Bi^{3+} ions.[45] In Bi-compounds, the dominant excitation transition is commonly ascribed to the population of the excited state $^3P_1$ from ground state $^1S_0$ (allowed by spin-orbit coupling), being the $^3P_0$ level strongly forbidden and a metastable state. At high temperatures, the emission $^1P_1 \rightarrow {}^1S_0$ transition is the most frequent in relation with $^3P_1 \rightarrow {}^1S_0$ transition, evidenced as broad bands accompanied with splitting components.[46]

Therein, the emission peaks of **Bi-1** are located in longer wavelength (446, 486 and 511 nm) compared to **Bi-2** (421, 435 and 464 nm) (Figure 11). The signal located at 511 nm in **Bi-1** could be attributed to $\pi \leftarrow \pi^*$ and/or $n \leftarrow \pi^*$ from 1,2,4,5-BTC and 2,2'-bipyridine ligands. For **Bi-2**, the contribution of the $n \leftarrow \pi^*$ transition from IDA carboxylate linker cannot be discarded. Moreover, it is remarkable that the band splitting between both spectra is different, meanwhile the intensities are similar. For an in-depth analysis, **Zn-1** was obtained and compared to **Bi-1**. Due to the fact that **Zn-1** and **Bi-1** have the same set of coordinated ligands, both compounds exhibit broad bands. The phosphorescence emitting bands were further analyzed by recording intensity decay curves (see SI section S11), and luminescence lifetimes were calculated by fitting mono-exponential functions, $I=A\cdot\exp(-t/\tau_{obs})$. The corresponding yielded τ_{obs} were 16.7 µs and 0.52 µs for **Bi-1**

View Article Online
DOI: 10.1039/C7DT04287F

and **Bi-2**, respectively. The τ_{obs} values of the Bi-CPs are higher compared to $Bi(NO_3)_3$, H_2IDA and H_4BTC (1.03, 1.32 and 1.02 ns respectively).

These differences might be related to their different coordination environment around Bi^{3+} ions[47], as Bi is nine-coordinated in **Bi-1**, while eight-coordinated in **Bi-2**. The SSPL and excitation spectra of both Bi-CPs suggest that two different emission metal center are responsible for the resultant luminescence components. It is noticeable that the two maximum in the excitation spectra are shifted by 30 nm, which is ascribed to the absorption of bismuth emitting center.

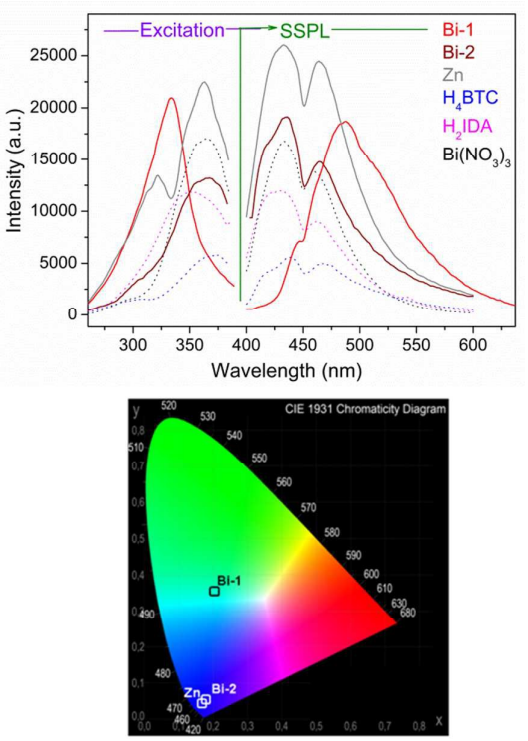

Figure 11: Top: Excitation (left) and emission (right) spectra of Bi-CPs in comparison with $Bi(NO_3)_3$, H_2IDA, H_4BTC and **Zn-1**. Down: Chromaticities (CIE 1931) exhibited by **Bi-1**, **Bi-2** and **Zn-1**.

The QC for optical materials enables to an accurate comparison between different materials related with its light-emitting performance. In this sense, the color coordinates are usually calculated employing the CIE (Commission International de L'Éclairage) system (SI section S12), proposed in 1931.[48] According to this approach, **Bi-1** and **Bi-2** were identified with bluish green and bluish purple emissions respectively (Figure 11 bottom). In comparison, similar colorimetric and spectroscopic features were observed in analogous Bi-HPyr (H_4Pyr=1,2,4,5-BTC) which exhibited pale green luminescence.[47] Basing on this analysis, **Bi-1** and **Bi-2** can be used as precursor materials for blue-light OLED/LEDs devices

4.5. Catalytic Activity

Cyanosilylation reactions (CSRs) are important carbon–carbon bond-forming processes that are catalyzed by Lewis acids/bases that can be used in homogeneous[49], or heterogeneous[50]. Among all the alternatives, MOFs and CPs are good choices in the heterogeneous catalysts for Lewis acid reactions owing to their unique reactivity and selectivity under mild reaction conditions.[8,10,13] So, taking into account the excellent Lewis acid activity displayed by several In-MOFs reported in the literature,[10,11,13] we decided to test the catalytic activity of **Bi-1**, **Bi-2** and **In-1** in the cyanosilylation of acetophenone (Table 1).

It was found that the reactivity changes as a function of the metal nature and the number of catalytic active sites presented in each structure. A study of the kinetic profile (Figure 12) was made, to understand the catalytic performance of each material and to determine their Turn Over Frequencies (TOFs) values.

The PXRD patterns of the recovered **Bi-2** and **In-1** after the catalytic reactions indicate that these materials do not suffer any structural change. However, **Bi-1** do not maintain its structural integrity after the catalytic reaction (see SI, section S13), and will be not considered as heterogeneous catalyst for further experiments.

Table 1. Screening of materials as catalysts for cyanosilylation reaction using acetophenone as carbonyl source.

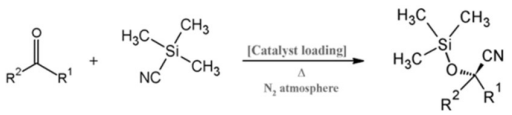

Material	Metal CN Dimensionality	Topology	Yield (%) [b] time (h)	TOF [c]	TON [d]
Bi-1[a]	9, 1D	Chain	86 (4)	184	86
Bi-2[a]	8, 1D	Chain	70 (4)	33	70
In-1[a]	6, 2D	**sql**	96(4)	76	96
In-1 [e]	6, 2D	**sql**	98 (4)	-	40
In-1 [f]	6, 2D	**sql**	90(6)	-	180
$InBr_3$ [g] [51]	Salt	-	90(3)	-	90
Blank	N.A	N.A	28(24)	N.A	N.A

[a] Solvent free reaction at 25ºC and 1 mol% of catalyst under N_2 atmosphere, [b] Yields (GC-MS), [c] TOF: $\Delta\chi$ x [mol of reactant / mol catalyst]/ Δt), [d] TON: (χ/ mol catalyst), [e] Reaction employing 2.5 mol% of catalyst loading, [f] Reaction employing 0.5 mol% of catalyst loading, [g] homogeneous catalyst [1 mol%] using CH_2Cl_2 as solvent.

View Article Online
DOI: 10.1039/C7DT04287F

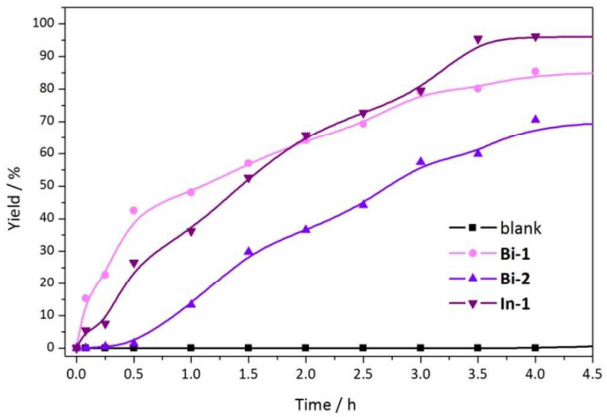

Figure 12: Kinetic profiles of **Bi-1, Bi-2** and **In-1** catalysts in the cyanosilylation of acetophenone.

From the data presented in Table 1 it is evident that a structure/catalytic ability relationship exits. The comparison between **Bi-2** and **In-1**, which have the same organic linker in their structure, allows the study based on the nature of the metal cation. It would be expected that Lewis acid behavior follows **In-1** > **Bi-2** order, based on the cation size impact in the acid strength. Besides indium catalyst with octahedral metal centers forms a covalent framework with higher dimensionality (2D layers) than **Bi-2** (1D chains) material. This higher covalent disposition of **In-1** clearly seems to favor the interaction between the available active sites of the catalyst with the substrates, even for the most sterically hindered ones, as can be appreciated in Table 2.

The scope of the reaction was studied for the cyanosilylation of ketones using **In-1** as catalyst (Table 2). In case of non-aromatic ketones (Table 2, entries 4-8), higher yields were obtained compared to the aromatic ones (Table 2, entries 1-3). Reactions with linear aliphatic ketones (Table 2, entries 7-8) proceeded efficiently giving the corresponding product at shorter times with yields over 85%. The cyclic ketones (Table 2, entries 4-6) higher yields were obtained (>97%). Finally, the less reactive aromatic ketones also reached good yields (80-96%).

Table 2. Scope of the **In-1** cyanosilylation of ketones.[a]

Entry	Ketone	time (h)	Yield (%)[b]	TON[c]
1	acetophenone	4	96	96
2	4-methylacetophenone	8	89	89
3	2-methylacetophenone	8	80	80
4	Cyclopentanone	3.5	98	98
5	cyclohexanone	4	96	96
6	4-methylcyclohexanone	4	97	97
7	2-hexanone	3	>99	99
8	3-hexanone	3	85	85

[a] Solvent free reaction at 25 ºC and 1 mol% of catalyst under N_2 atmosphere, [b] product Yields (GC-MS) and [c] TON: (χ/ mol catalyst).

The results of the reactions carried out with acetophenone derivatives with electron-donating substituents such as 2-methylacetophenone and 4-methylacetophenone, showed yiels of 80% and 89% respectively.

The recyclability tests shows that **In-1** material maintains its crystallinity even after ten catalytic cycles, with only a small decrease of its catalytic activity, probably due to the losses during the recovery of the catalyst (see SI, section S14). Hot filtration experiments reveal that **In-1** is a truly heterogeneous catalyst.

4.6. Antibacterial assays

Firstly, effects of Bi-NPs and Bi-cit on the cell growth of planktonic cultures of *E. coli*, S. Typhimurium and *P. aeruginosa*, were analyzed. Figure 13 shows that **Bi-1** required 1.2 μg·ml^{-1} to decrease 6 logs in *E. coli* and *P. aeruginosa* and 7 logs in *S. Typhimurium* (viable counts compared to controls). In contrast, 295 μg·ml^{-1} of **Bi-2** were required to reduce 2 logs the cell viability of *E. coli* and *S. Typhimurium*, and 4 logs in *P. aeruginosa* (Figure 13b). Bi-cit decreased cell viability 1.5-2 logs at 6.8 μg·ml^{-1} in all the studied microorganisms (Figure 13). Reduction of cell mass measured by OD_{650} followed the same observed tendency for the cell viability (Figure 13). According to these results, the greatest effect was produced by **Bi-1**, not only for the several orders of log reduction, but also by the lower concentration required for reduction of bacterial growth (Table 3).

Table 3: Log_{10} reductions of bacterial viability produced by Bi-compounds compared to controls, according to the maximum concentration of compound used.

Organism	**Bi-1** (1.2 μg/ml)	**Bi-2** (295 μg/ml)	Bi-cit (6.8 μg/ml)
E. coli	6	2	2
S. Typhimurium	7	2	2
P. aeruginosa	6	4	1.5

View Article Online
DOI: 10.1039/C7DT04287F

Then the effect of Bi-NPs on biofilm formation of *P. aeruginosa* was studied. *P. aeruginosa* is a relevant opportunistic pathogen of humans; given its great capacity to form biofilms on diverse surfaces causing severe damages to industry and human health, it is largely employed as model in biofilm studies. Quantification of biofilms in control and test assays demonstrated that both Bi-NPs efficiently inhibited biofilm formation, although **Bi-1** produced its antibiofilm effect at lower concentrations than **Bi-2** (Figure 14a). In contrast to Bi-NPs, Bi-cit did not inhibit biofilm formation at concentrations ≤ 3 μg/ml; moreover, it promoted its development. However, at higher concentrations, this effect was reversed and inhibition of biofilm formation was observed. Representative images of stained 24 h biofilms illustrate the inhibitory effect of Bi-NPs on biofilm formation (Figure 14b). It is concluded that both Bi-NPs are effective antibiofilm agents in *P. aeruginosa*, being **Bi-1** more powerful than **Bi-2**.

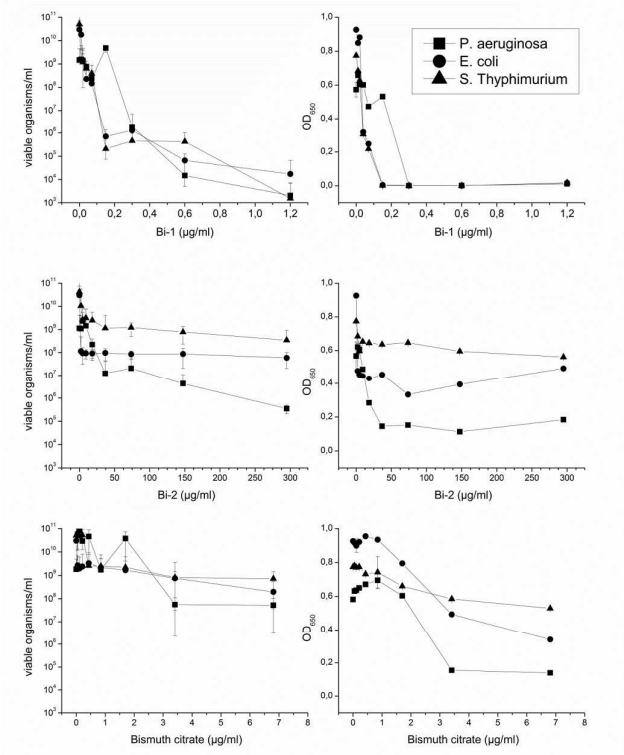

Figure 13: Viable organisms/mL and OD_{650} profiles of **Bi-1**, **Bi-2** and Bi-cit.

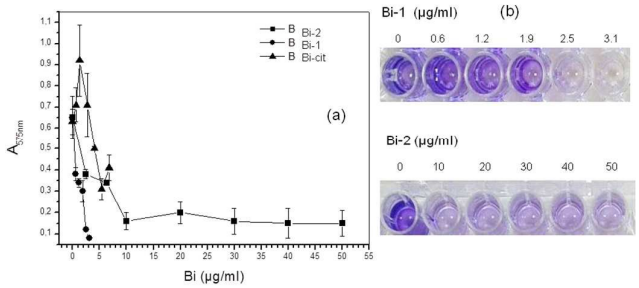

Figure 14: Effect of Bismuth compounds on biofilm formation in *P. aeruginosa* (a). *P. aeruginosa* was grown in 96 well microplates in absence or in presence of different concentrations of Bi-NPs and Bismuth citrate. Biofilms adhered to the wells were subsequently stained with crystal violet and the absorbance of the solubilized stain was measured at 575 nm. Error bars represent the standard deviation of at least three independent experiments (b). Visualization of biofilm formation in absence or in presence of different concentrations of Bi-NPs by crystal violet staining. Representative images are shown.

Conclusions

A set of CPs based on bismuth, indium and zinc were successfully obtained. Due to the lack of studies regarding to structural, optical, mechanical and antibacterial properties of CPs an exhaustive analysis covering these topics was carried out. These compounds were synthesized from bismuth and indium salts, IDA, 1,2,4,5-BTC, and 2,2'-bipyridine as building blocks. The one-dimensional Bi-CPs, $[Bi(1,2,4,5\text{-}BTC)_{0.5}(2,2'\text{-bipyridine})(NO_3)(DMF)]$ and [Bi(IDA)(IDAH)], belonged to $P\bar{1}$ and C2/*c* space groups, meanwhile the layered In-CP, [In(IDA)Cl], belonged to the Pnma space group. Moreover, an in-deep analysis of the topology was carried out, where the Bi-CPs were simplified as "ribbon-like" chains, and **sql**/Shubnikov tetragonal plane net with point symbol $(4^4.6^2)$.

In order to find relationships between the structural features and the intrinsic mechanical properties, nanoindentation studies were performed onto a 1D and a layered compound (**Bi-2** and **In-1**). The differences in the mechanical performances in both compounds were related to their crystal packing. According to H and E values, the CPs were located into the "dense hybrids" type materials. These studies are important to evaluate the mechanical qualities in low dimensional materials for device development.

The SSPL properties of the Bi-CPs were studied, which involved excitation–emission, lifetime experiments and quantification of colour emission. Regarding to these results, the Bi-CPs were classified as blue-emitters in the visible region, with performances compared with analogous Bi-compounds and TM-MOFs. These optical features made Bi-CPs important for the design of photonic devices with blue light emissions.

From our catalytic studies under solvent-free conditions on these new CPs we can conclude that the factor which drives the reaction yield relies on the metal nature and framework

View Article Online
DOI: 10.1039/C7DT04287F

dimensionality. Therefore, the catalytic activity decreases in the following order **In-1**>**Bi-2**. **In-1** material is capable of work as a real heterogeneous catalyst, using several hindered carbonyl derivates at mild reaction conditions reaching high yields with a good recyclability rate.

Finally, the strong antibacterial effect of the Bi-CPs on *E. coli*, Typhimurium, S. Typhimurium and *P. aeruginosa*, was observed and compared to the well known bismuth salt Bi-cit, especially in the case of **Bi-1**. The emergence and spread of antibiotic resistant derivatives constitute an actual problem that threatens the efficacy of treatment of many bacterial infections with antibiotics, then it is necessary the development of novel pathogen eradication methodologies.

Conflicts of interest

There are no conflicts to declare.

Acknowledgements

This work was supported by the Consejo Nacional de Investigaciones Científicas y Técnicas, ANPCyT PICT 2012-2087 and CNEA. G. E. G. acknowledges the postdoctoral CONICET fellowship and HYMADE project. R. D. acknowledges Coordenação de Aperfeiçoamento de Pessoal de Nível Superior for the CAPES/PNPD scholarship from the Brazilian Ministry of Education and Universidad Santiago de Cali. D. F. L. acknowledges doctoral CONICET fellowship. Ramón Castillo Guerra, Ricardo Montero, Guillermo Arnaldo, Rodrigo Taboada and Gonzalo Zbihlei, from Departamento de Materiales – (CNEA), are gratefully thanked for helping with sample preparation for NI testing. L. M. A.-D., M. I. and M. A. M. acknowledge the Spanish Ministry of Economy, Industry and Competitiveness (MINECO-Spain) projects MAT2013-45460-R, MAT2014-52085-C2-2-P, MAT2016-78465-R and CTQ2014-61748-EXP, Fondo Social Europeo from the European Union. Comunidad Autónoma de Madrid S2013/MIT-2740 (PHAMA 2.0). R. V. D. and A. M. K. acknowledge Ghent University's Special Research Fund (BOF) for a Posdoctoral Mandate (project BOF15/PDO/091). J. E. is grateful to CNPq for the research fellowships. G. J. A. A. S. I. and M. C. F. are members of CIC-CONICET. Besides, this project has received funding from the European Union's Horizon 2020 research and innovation program H2020-MSCA-RISE-2014, GA Nº 645686.

References

1 N. L. Rosi, J. Eckert, M. Eddaoudi, D. T. Vodak, J. Kim, M. OKeeffe and O. M. Yaghi, *Science*, 2003, **300**, 1127.
2 J. Heine, K. Müller-Buschbaum, *Chem. Soc. Rev*., 2013, **42**, 9232.
3 (a) J. -L. Wang, C. Wang and W. Lin, *ACS Catal.*, 2012, **2**, 2630; (b) A. Corma, H. García and F. X. Llabrés i Xamena, *Chem. Rev*., 2010, **110**, 4606.
4 (a) A. Thirumurugan, A. K. Cheetham, *Eur. J. Inorg. Chem*. 2010, 3823. (b) A. Thirumurugan, J.-C. Tan, A. K. Cheetham, *Cryst. Growth Des*., 2010, **10**, 1736; (c) A. C. Wibowo, S. A. Vaughn, M. D. Smith, H.-C. zur Loye, *Inorg. Chem*., 2010, **49**, 11001; (d) A. C. Wibowo, M. D. Smith, H.-C. zur Loye, *CrystEngComm*, 2011, **13**, 426; (e) A. Thirumurugan, W. Li, A. K. Cheetham, *Dalton Trans*., 2012, **41**, 4126, (f) Liang Kan, Jiantang Li, Xiaolong Luo, Guanghua Li, Yunling Liu, *Inorg. Chem. Comm*., doi.org/10.1016/j.inoche.2017.06.018.
5 M. Feyand, E. Mugnaioli, F. Vermoortele, B. Bueken, J. M. Dieterich, T. Reimer, U. Kolb, D. de Vos and N. Stock, *Angew. Chem*., 2012, **124**, 10519; (b) M. Feyand, E. Mugnaioli, F. Vermoortele, B. Bueken, J. M. Dieterich, T. Reimer, U. Kolb and D. de Vos, N. Stock, *Angew. Chem. Int. Ed*., 2012, **52**, 10373.
6 (a) G. E. Gomez, M. C. Bernini, E. V. Brusau, G. E. Narda, W.r A. Massad and A. Labrador, *Cryst. Growth Des.*, 2013, **13**, 5249; (b) R. F. D'Vries, G. E. Gomez, J. H. Hodak and G. J. A. A. Soler-Illia, J. Ellena, *Dalton Trans*., 2016, **45**, 646; (c) G. E. Gomez, M. C. Bernini, E. V. Brusau, G. E. Narda, D. Vega, A. M. Kaczmarek, R. Van Deun and M. Nazzarro, *Dalton Trans*., 2015, **44**, 3417.
7 R. F. D'Vries, G. E. Gomez, D. F. Lionello, M. C. Fuertes, G. J. A. A. Soler-Illia and J. Ellena, *RSC Adv*., 2016, **6** (111), 110171.
8 G. E. Gomez, A. M. Kaczmarek, R. Van Deun, E. V. Brusau, G. E. Narda, D. Vega, M. Iglesias, E. Gutierrez-Puebla and M. Ángeles Monge, *Eur. J. Inorg. Chem*., 2016, **2016 (10)**, 1577.
9 R. F. D'Vries, V. A. de la Peña-O'Shea, N. Snejko, M. Iglesias, E. Gutiérrez-Puebla and M. A. Monge, *J. Am. Chem. Soc.*, 2013, **135**, 5782.
10 (a) L. M. Aguirre-Díaz, D. Reinares-Fisac, M. Iglesias, E. Gutiérrez-Puebla, F. Gándara, N. Snejko, M. A. Monge, *Coord. Chem. Rev.,* 2017, **335**, 1. (b) L. M. Aguirre-Díaz, M. Iglesias, N. Snejko, E. Gutiérrez-Puebla and M. A. Monge, *RSC Adv*., 2015, **5**, 7058.
11 (a) R. F. D'Vries, Susana Álvarez-García, Natalia Snejko, Luisa E. Bausá, Enrique Gutiérrez-Puebla, Alicia de Andrés and M. A. Monge, *J. Mat. Chem. C*, 2013, **1(39)**, 6316. (b) R. F. D'vries, M. Iglesias, N. Snejko, E. Gutiérrez-Puebla, M. A. Monge, *Inorg. Chem*., 2012, **51**, 11349-11355.
12 (a) G. E. Gomez, E. V. Brusau, A. M. Kaczmarek, C. Mellot-Draznieks, J. Sacanell, G. Rousse, R. Van Deun, C. Sanchez, G. E. Narda and G. J. A. A. Soler Illia, *Eur. J. Inorg. Chem*., 2017, **2017 (17)**, 2321. (b) A. A. Godoy, G. E. Gomez, A. M. Kaczmarek, R. Van Deun, O. J. Furlong, F. Gándara, M. A. Monge, M. C. Bernini, G. Narda, *J. Mater. Chem. C*, 2017, **5**, 12409-12421.
13 (a) L. M. Aguirre-Díaz, F. Gándara, M. Iglesias, N. Snejko, E. Gutiérrez-Puebla and M. A. Monge, *J. Am. Chem. Soc*., 2015, **137,** 6132. (b) L. M. Aguirre-Díaz, M. Iglesias, N. Snejko, E. Gutiérrez-Puebla and M. A. Monge, *Chem. Eur. J.* 2016, **22**, 6654. (c) D. Reinares-Fisac, L. M. Aguirre-Díaz, M. Iglesias, N. Snejko, E. Gutiérrez-Puebla, M. A. Monge and F. Gándara, *J. Am. Chem. Soc*., 2016, **138 (29)**, 9089.
14 A. K. Inge, M. Köppen, J. Su, M. Feyand, H. Xu, X. Zou, M. O'Keeffe and N. Stock, *J. Am. Chem. Soc*., 2016, **138**, 1970.
15 (a) X. X. Wang, B. Yu and K. Van Hecke, *RSC Adv*., 2014, **4(106)**, 61281-61289. (b) J.-M. Hao, L. N. Wang, K. Van Hecke, G.-H. Cui, *Inorg. Chem. Comm*., 2014, **41**, 43-46. (c) J.-M. Hao, B.-Y. Yi, K. Van Hecke, G.-H. Cui, *CrystEngComm*, 2015, **17**, 2279-2293. (d) L.-M. Zhang, D.-Y. Deng, G. Peng, L. Liang, G.-Q. Lan, H. Deng, *CrystEngComm*., 2012, **14**, 8083-8089.
16 G. R. Rudramurthy, M. K. Swamy, U. R. Sinniah and A. Ghasemzadeh, *Molecules*, 2016, **21**, 836.
17 (a) D. Mahony, S. Lim-Morrison, L. Bryden, G. Faulkner, P. Hoffman, L. Agocs, G. Briand, N. Burford and H. Maguire, *Anti. Ag. and Chemotherapy*, 1999, **43**, 582; (b) J. R. Lambert, *Reviews of Infectious Diseases*, 1991, **13**, 691; (c) M. D. Manhart, *Reviews of Infectious Diseases*, 1990, **12**, 11. (d) A. M Pitz, G. W Park, D. Lee, Y. L. Boissy and J. Vinjé, *Gut*

View Article Online
DOI: 10.1039/C7DT04287F

Microbes, 2015, **6:2**, 93. (e) D. M. Keogan and D. M. Griffith, *Molecules* **2014**, 19, 15258.
18 C. Cabral, C. Shankararaman, 2014. Bismuto nanoparticles: antimicrobials of broad spectrum, low cost and safety. In Nanomedicine, chap. *17*, 430. Eds: A Seifalian, A de Mel and D M Kalaskar. Publisher One Central Press (OCP).
19 R. Hernández-Delgadillo, D. Velasco-Arias, D. Diaz, Zerovalent bismuto nanoparticles inhibit Streptococcus mutans growth and formation of biofilm. Int J Nanomedicine 7:2109-2113.
20 R. Hernández, D. Velasco, J. J. Martínez, D. Diaz, I. Zumeta, K. Arevalo and C. Cabral, *Inter. Journal of Nanomedicine*, 2013, **8**, 1645.
21 (a) A. Rajasekar, B. Anandkumar, S. Maruthamuthu, Y. P Ting and P. K. S. M. Rahman, *Appl. Microbiol. Biotechnol*., 2010, **85**, 1175. (b) P. Gupta, S. Sarkar, B. Das, S. Bhattacharjee, P. Tribedi, *Arch Microbiol*., 2016, **198**, 1. (c) T.- F. C. Mah and G. A. O'Toole, *Trends Microbiol.,* 2001, **9**, 34.
22 J. C. Tan, J. D. Furman and A. K. Cheetham, *J. Am. Chem. Soc*., 2009, **131**, 14252.
23 CrystalClear; 2.0 ed.; Rigaku Corporation: Tokyo, Japan, 2005.
24 CrysAlisPro; Ltd, A. T., Ed.; Agilent Technologies Ltd: Yarnton, Oxfordshire, England, **2014**.
25 Sheldrick, G. Acta Crystallographica Section A **2008**, 64, 112.
26 Farrugia, L. *J. Appl. Crystallogr.,* 2012, **45**, 849.
27 O. V. Dolomanov, L. J. Bourhis, R. J. Gildea, J. A. K. Howard and H. Puschmann, *J. Appl. Crystallogr.* 2009, **42**, 339.
28 Bruker-AXS, I.; 2 ed. Madison, WI, 2006.
29 Brandenburg, H. P. K. In *DIAMOND*; Impact, C., Ed.; Crystal Impact: Kreuzherrenstr. 102, 53227 Bonn, Germany, **2006**.
30 V. A. Blatov, A. P. Shevchenko, D. M. Proserpio, *Crystal Growth & Design,* 2014, **14**, 3576.
31 C. F. Macrae, I. J. Bruno, J. A. Chisholm, P. R. Edgington, P. McCabe, E. Pidcock, L. Rodriguez-Monge, R. Taylor, J. Van De Streek, P. A. Wood, *J. Appl. Crystallogr.,* 2008, **41**, 466.
32 J. H. Merritt, D. E. Kadouri, G. A. O'Toole, *Curr. Protoc. Microbiol.* Unit 1B.1 2005, 1B.1.1-1B.1.17.
33 N. G. Connelly, T. Damhus, R.M. Hartshorn and A.T. Hutton, *Nomenclature of Inorganic Chemistry - IUPAC Recommendations 2005*; RSC Publishing: Cambridge, UK., 2005.
34 (a) E. V. Alexandrov, V. A. Blatov, A. V. Kochetkov and D. M. Proserpio, *CrystEngComm*, 2011, **13**, 3947; (b) M. O'Keeffe, O. M. Yaghi, *Chem. Rev.*, 2012, **112**, 675.
35 A. K. Cheetham, C. N. R. Rao and R. K. Feller, *Chem. Commun*. 2006, 4780.
36 R. Prajapati, L. Mishra, K. Kimura and P .Raghavaiah, *Polyhedron,* 2009, **28**, 600.
37 X. Xu, Y. Lu, E. Wang, Y. Ma and X. Bai, *J. Mol. Struct.,* 2006, **825**, 124.
38 (a) F. Mammeri, E. Le Bourhis, L. Rozes, C. Sanchez, *J. Mater. Chem.*, 2005, **15**, 3787. (b) D. Zacher, O. Shekhah, C. Woll and R. A. Fischer, *Chem. Soc. Rev.*, 2009, **38**, 1418. (c) R. Ameloot, L. Stappers, J. Fransaer, L. Alaerts, B. F. Sels and D. E. De Vos, *Chem. Mater*., 2009, **21**, 2580. (d) A. S. Huang, H. Bux, F. Steinbach and J. Caro, *Angew. Chem., Int. Ed*., 2010, **49**, 4958.
39 Yuan Peng, Yanshuo Li, Yujie Ban, Hua Jin, Wenmei Jiao, Xinlei Liu and Weishen Yang, *Science*, 2014, **346**, 1356.
40 Jin-Chong Tan, Paul J. Saines, Erica G. Bithell and Anthony K. Cheetham, *ACS Nano*, 2012, **6**, 615.
41 J. C. Tan, C. A. Merrill, J. B. Orton and A. K. Cheetham, *Acta Mater*., 2009, **57**, 3481.
42 J. C. Tan and A. K. Cheetham, *Chem. Soc. Rev*., 2011, **40**, 1059.
43 (a) R. F. D'Vries, M. Iglesias, N. Snejko, S. Alvarez-Garcia, E. Gutierrez-Puebla and M. A. Monge, *J. Mater. Chem*., 2012, **22**, 1191. (b) R. Decadt, K. Van Hecke, D. Depla, K. Leus, D. Weinberger, I. Van Driessche, P. Van Der Voort and R Van Deun, *Inorg. Chem.,* 2012, **51**, 11623. (c) D. Esquivel, A. M. Kaczmarek, C. Jiménez-Sanchidrián, R. Van Deun, F. J. Romero-Salguero, P. Van Der Voort, *J. Mater. Chem. C*, 2015, **3**, 2909.
44 A. Vogler and H. Nikol, *Pure Appl. Chem.*, 1992, **64**, 1311.
45 X. H. Yu, H. H. Zhang, Y. N. Cao, Y. P. Chen and Z. Wang, *J. Solid State Chem.*, 2006, **179**, 247
46 (a) D. M. A. Ranfagni, M. Bacci, G. Viliani and P. Fontana, *Adv. Phys*., 1983, **32**, 823; (b) J.-G. Kang, H.-M. Yoon, G.-M. Chun, Y.-D. Kim, T. Tsuboi, *J. Phys. Condens. Matter*, **1994**, 6, 2101.
47 M. Feyand, M. Köppen, G. Friedrichs and N. Stock, *Chem. Eur. J.*, 2013, **19**, 12537.
48 G. Kickelbick, in Hybrid Materials, Wiley-VCH Verlag GmbH & Co. KGaA, 2007, pp. 1-48.
49 (a) B. Y. Park, K. Y. Ryu, J. H. Park, S.-g. Lee, *Green Chem*., 2009, **11**, 946. (b) N. Kurono, M. Yamaguchi, K. Suzuki, T. Ohkuma, *J. Org. Chem*., 2005, **70**, 6530. (c) P. Saravanan, R. V. Anand, V. K. Singh, *Tetrahedron Lett.*, 1998, **39**, 3823.
50 (a) Y. Ogasawara, S. Uchida, K. Yamaguchi, N. Mizuno, *Chem. Eur. J.*, 2009, **15**, 4343 (b) A. Procopio, G. Das, M. Nardi, M. Oliverio, L. Pasqua, *ChemSusChem*, 2008, **1**, 916 (c) K. Iwanami, J.-C. Choi, B. Lu, T. Sakakura, H. Yasuda, *Chem. Commun.*, 2008, 1002.
51 M. Bandini, P. Cozzi, A. Garelli, P. Melchiorre, A. Umani-Ronchi, *Eur. J. Org. Chem*., 2002, 3243.

Graphical abstract